CMS Physics Analysis Summary

Contact: cms-pag-conveners-ewk@cern.ch 2012/03/09

Forward-backward asymmetry of Drell-Yan pairs

The CMS Collaboration

Abstract

We present a measurement of the forward-backward asymmetry (A_{FB}) for opposite charge lepton pairs produced via an intermediate Z/γ^* at $\sqrt{s} = 7$ TeV in the CMS experiment. Our results are based on an integrated luminosity of 4.7 fb^{-1}. We present A_{FB} as a function of the di-lepton mass for $M_{\ell^+\ell^-} > 40$ GeV, the raw A_{FB} for both di-muons and di-electrons and the combined measurement at the Born level. The di-muon channel and the combined A_{FB} measurements represent the first such measurements at a hadron collider. We find that the A_{FB} distributions are consistent with the Standard Model predictions within uncertainties.

1 Introduction

In the Standard Model (SM) process $q\bar{q} \rightarrow Z/\gamma^* \rightarrow \ell^+\ell^-$, both the vector and axial-vector couplings of electroweak bosons to fermions are present. This results in a forward-backward asymmetry ($A_{\rm FB}$) in the number of Drell-Yan pairs. At a given di-lepton invariant mass, the differential cross-section can be written as

$$\frac{d\sigma}{d(\cos\theta)} = A(1+\cos^2\theta) + B\cos\theta \tag{1}$$

where θ is the emission angle of the lepton relative to the quark momentum in the center-of-mass frame of the di-leptons, and A and B are parameters that depend on the weak isospin and the charge of the quark and the anti-quark. Forward (backward) events are defined by $\cos\theta > 0$ (< 0). The total cross sections for the forward ($\sigma_{\rm F}$) and backward events ($\sigma_{\rm B}$) are then

$$\begin{aligned}\sigma_{\rm F} &= \int_0^1 \frac{d\sigma}{d(\cos\theta)} d(\cos\theta) = A\left(1+\frac{1}{3}\right) + B\left(\frac{1}{2}\right) \\ \sigma_{\rm B} &= \int_{-1}^0 \frac{d\sigma}{d(\cos\theta)} d(\cos\theta) = A\left(1+\frac{1}{3}\right) - B\left(\frac{1}{2}\right)\end{aligned} \tag{2}$$

and the asymmetry parameter, $A_{\rm FB}$, is simply

$$A_{\rm FB} = \frac{\sigma_F - \sigma_B}{\sigma_F + \sigma_B} = \frac{3B}{8A}. \tag{3}$$

At the Z pole $A_{\rm FB}$ is small, due to the small value of the lepton vector coupling constant, and provides a measurement of $\sin^2\theta_W$ [1]. Above and below the Z pole, $A_{\rm FB}$ exhibits a characteristic energy dependence, driven by virtual photon and Z interference. Precision measurements of $A_{\rm FB}$ can be used to constrain Parton Distribution Functions (PDFs), and substantial deviations from the SM prediction of $A_{\rm FB}$ may indicate the existence of a new neutral gauge boson [2–7], quark-lepton compositeness [8], supersymmetric particles or extra dimensions [9]. Initial studies of the forward-backward asymmetry in CMS using Monte Carlo (MC) samples are described in references [10, 11] and the preliminary measurement of $A_{\rm FB}$ in the di-muon and di-electron channels in [12–14].

In this paper, we use the Collins-Soper frame [15] in which the angle θ^*_{CS} is defined as the angle between the lepton momentum and an axis that bisects the angle between the quark and opposite to the anti-quark direction. Use of this frame reduces the uncertainties due to the transverse momentum of the incoming quarks. The angle θ^*_{CS} can be calculated using quantities measured in the lab frame as

$$\cos\theta^*_{CS} = \hat{Q}_Z \frac{2(P_l^+ P_{\bar{l}}^- - P_l^- P_{\bar{l}}^+)}{|Q|\sqrt{Q^2 + Q_T^2}} \tag{4}$$

where Q, Q_T and Q_Z are the four-momentum, the transverse momentum, and the longitudinal momentum of the di-lepton pair. $P_l(P_{\bar{l}})$ represents the four momenta of the lepton (anti-lepton), and $P_l^\pm = 2^{-1/2}(P_l^0 \pm P_l^3)$. At the LHC, the quark direction can not be known since both beams consist of protons. However, since the anti-quark is necessarily a sea quark, on average, we expect it to carry less momentum than the valence quark and therefore, the di-lepton system should be boosted in the direction of the valence quark [3, 16, 17]. This assumption is taken into account by including the sign of the Z boost ($\hat{Q}_Z$) in the definition of $cos\theta^*_{CS}$ in Equation 4.

The raw $A_{\rm FB}$ measurement is distorted compared to the parton-level asymmetry mainly because of bin-to-bin migration in mass due to the finite mass resolution of the detector and the QED Final-State-Radiation (FSR). Moreover, $A_{\rm FB}$ is further distorted by the acceptance cuts and the unknown quark directions at the LHC. In this paper, we present the uncorrected $A_{\rm FB}$ and compare it to the reconstructed POWHEG events. We also present the $A_{\rm FB}$ corrected for the mass resolution and QED FSR effects (Born level).

We calculate the $\cos\theta$ distributions in $M-Y$ bins the limits of which are defined to be M = 40, 50, 60, 70, 80, 86, 96, 106, 120, 150, 200, 2000 GeV and $|Y|$ = 0, 1, 1.25,1 .5, and 2.4. To correct for mass resolution and QED FSR effects, we unfold the forward and backward mass spectra in each Y-bin. The unfolding procedure is performed using a matrix inversion technique.

$A_{\rm FB}$ could be further corrected for the dilution effects due to unknown quark direction. However, such corrections use information that are not directly observable and beyond the scope of the measurement. Dilution corrections can be made by theorists using the unfolded $A_{\rm FB}$ presented in this paper.

2 Detector, Data and Monte Carlo Samples

A detailed description of the CMS detector can be found in [18]. The central feature of the CMS detector is a 3.8 T superconducting solenoid of 6 m internal diameter. The Silicon Pixel and Strip Tracker, the Crystal Electromagnetic Calorimeter (ECAL) and the Brass/Scintillator Hadron Calorimeter (HCAL) are located inside the solenoid. In CMS, muons are measured in the pseudorapidity window $|\eta|$ <2.4, with the all-silicon Tracker and the Muon System with detection planes of three technologies embedded in the steel return yoke: Drift Tubes (DT), Cathode Strip Chambers (CSC), and Resistive Plate Chambers (RPC) [19]. DTs are used in the barrel ($|\eta|$ <1.2), and CSCs in the endcaps (0.9< $|\eta|$ <2.4), complemented by a system of RPCs covering both regions up to $|\eta|$ <1.6. Electrons are detected in ECAL as energy clusters and as tracks in the Silicon Tracker. ECAL consists of nearly 76 000 lead tungstate crystals which provide coverage in pseudorapidity $|\eta| < 1.479$ in the barrel region (EB) and $1.479 < |\eta| < 3.0$ in the two endcap regions (EE). A preshower detector consisting of two planes of silicon sensors interleaved with a total of 3 X_0 of lead is located in front of the EE.

This analysis is based on 4.7 fb^{-1} of data at 7 TeV center-of-mass energy collected in 2011.

The signal ($Z/\gamma^* \rightarrow \mu^+\mu^-, e^+e^-$) and the $Z \rightarrow \tau\tau$ processes, considered as a part of background in this analysis, have been simulated using POWHEG at the Next-to-Leading-Order (NLO) [20–22]. Parton showering is simulated using PYTHIA [23] while the NLO PDF is CT10 [24]. The W+jets and $t\bar{t}$ background events are generated using MadGraph [25], PYTHIA and TAUOLA [26]. Background event samples WW, WZ, ZZ, and QCD are generated using PYTHIA. All events are processed and reconstructed using the GEANT4 based CMS software [27, 28].

3 Event Reconstruction and Selection

Muon candidates are selected from events with at least two muons with transverse momenta (p_T) of at least 6 or 7 GeV and the sub-leading muon with 8 GeV and the leading muon with 13 or 17 GeV depending on the period of data-taking. In the offline analysis, the muon tracks are first independently reconstructed by the Tracker and the Muon System. Muon candidates are then reconstructed by two different algorithms. The global muon algorithm matches the tracks in the Tracker to the tracks in the Muon System, and then refits the individual hits in Tracker

and Muon System to one overall track. The Tracker muon algorithm, on the other hand, extrapolates the tracks with $p_T > 0.5$ GeV and $p > 2.5$ GeV in the Tracker to the Muon System, and a track is taken to be a muon candidate if it matches at least one track segment in the Muon System. Both algorithms take into account the energy loss and multiple scattering in the steel yoke of the CMS magnet. High-quality muons are selected by the standard CMS muon identification cuts which require 10 hits in the Tracker, including one in the pixel detector, at least one hit in the Muon System, hits in at least two muon stations, and a normalized $\chi^2 < 10$ for the global fit. Muons are required to have a small impact parameter of less than 2 mm measured with respect to the beam spot. This requirement reduces the cosmic muon background significantly. We also require the angle between the two muon tracks to be larger than 2.5 mrad in the laboratory frame, which removes any remaining cosmic ray background without removing signal events. To remove muons overlapping with jets, they are required to pass the isolation that uses the sum of the transverse momenta of the tracks in the Tracker. The muon definition does not include the energy of the radiated photons, therefore, to reduce the effects of the QED FSR which is detected in the ECAL, isolation is defined only using Tracker information. For each muon we require $|\eta| \leq 2.4$ and $p_T > 20$ GeV.

Online electron candidates are selected from ECAL L1-triggered events by a high-level trigger requiring two ECAL clusters with a minimum E_T. Reconstruction of electrons starts by building superclusters of clusters in the ECAL in order to collect the energy radiated by bremsstrahlung in the Tracker material, following the procedure described in Ref. [29]. A dedicated tracking algorithm is used to better cope with the changes of curvature due to bremsstrahlung. Superclusters are then matched to electron tracks. Electron candidates are required to be in the pseudo-rapidity ranges $|\eta| \leq 1.444$ or $1.566 < |\eta| < 2.400$ with the minimum supercluster E_T of 20 GeV after ECAL energy scale corrections. Electrons from photon conversions are reduced by requiring no missing Tracker hits before the first hit in the reconstructed track matched to the electron and also by rejecting the candidate when a conversion partner track is found close to the electron candidate. High quality electrons are identified by using shower shape variables, and electron candidates are isolated using a variable that combines the Tracker and calorimeter measurements. Energy scale, resolution and efficiency factors are calculated and applied for different data-taking periods, η and p_T. The MC signal sample is re-weighted to mimic the pile-up conditions in the data.

Note that electrons are restricted to the same phase space of the muons for an unambiguous comparison and combination of the two channels.

For both channels, the main sources of background are $Z \to \tau\tau$ and QCD dijets for the low mass and $t\bar{t}$ for the high mass region. Diboson (WW, WZ, ZZ), and W inclusive processes are lesser sources of background. QCD may be a major background contribution in the di-electron channel depending on how often a jet is counted as an electron and passes the electron ID cuts. Electroweak (EW) backgrounds are calculated using MC samples, and the QCD background is estimated using a data-driven method in which we assume that the same-sign and the opposite-sign electron pairs are equally probable since the reconstruction of a charged particle in a jet to be counted as a lepton or anti-lepton is equally likely.

4 The Analysis

There are no geometrical or kinematic acceptance corrections in this analysis. All results are given in the phase-space defined by $p_T(\ell) > 20$ GeV and $|\eta(\ell)| < 2.4$. The dilution due to the unknown quark direction is largest for small rapidity values and decreases with increasing rapidity. The first rapidity bin, $|Y| = 0.00 - 1.00$ is the bin with the largest dilution effect due

to the unknown quark direction but with the smallest acceptance effect. The next two bins, $|Y| = 1.00 - 1.25$ and $|Y| = 1.25 - 1.50$, have the largest asymmetry. The highest rapidity bin, $|Y| = 1.5 - 2.4$, is affected the least by dilution but suffers a large acceptance reduction resulting in a smaller asymmetry compared to the adjacent Y bin.

The response matrix provides a mapping between the corrected and the measured number of events in each mass and rapidity bin. This is described by

$$N_j^{meas}(F,k) = \sum_{i=1}^{10} R_{ji}^{FF}(k) N_i^{corrected}(F,k) \qquad j = 1,...,10; k = 1,...,4. \tag{5}$$

$$N_j^{meas}(B,k) = \sum_{i=1}^{10} R_{ji}^{BB}(k) N_i^{corrected}(B,k) \qquad j = 1,...,10; k = 1,...,4. \tag{6}$$

In these equations, $N_j(F,k)$ and $N_j(B,k)$ refer to the number of forward (F) and backward (F) events within the acceptance ($p_T > 20$ GeV and $|\eta| < 2.4$) in each mass bin j for the rapidity bin k. $R_{ji}^{FF}(k)$ is the response matrix representing the effect that the observed mass bin is not always the generated mass bin for defined for forward events in the rapidity bin k and $R_{ji}^{BB}(k)$ is the response matrix for the backward events in the rapidity bin k. We construct the response matrices for unfolding the reconstructed forward and backward mass spectra in each Y bin to the Born level. The response matrices are calculated using the simulated events at the generator level before and after QED FSR and detector simulation. The response matrices that represent the forward generated but backward reconstructed events (and vice versa) have a negligible contribution and are neglected in this study. The effect of this approximation is taken into account in the systematic errors. The unfolded values are obtained by inverting the above equations. The corresponding errors are calculated taking into account the correlations that are due to the unfolding procedure. The estimated errors are verified applying the procedure on a large number of independent MC samples.

5 Systematic Uncertainties

Systematic uncertainties are estimated for each $M - Y$ bin using MC events and are calculated separately for the raw and the Born levels. To calculate the systematic uncertainties at the raw level, the MC distributions are modified, and the resulting $A_{\rm FB}$ values are compared to the nominal ones. To calculate the systematic uncertainties at the Born level, the modified MC distributions are unfolded, and the resulting $A_{\rm FB}$ values are compared to the nominal distributions at the Born level. All systematic uncertainties are assumed independent and combined in quadrature.

The background is small in the Drell-Yan process, however uncertainties in the background estimation lead to systematic errors in the final results. We take a conservative approach and assume that this small background is uncertain by 100%. We scale the background up and down by 100% and repeat the analysis.

To quantify possible systematic errors that could arise from the modeling of QED FSR, we re-weight the events in the FSR tail. We define the events in the FSR tail to be the events for which the difference of the momenta of the lepton pre- and post-radiation is larger than 1 GeV. We modify the weight of each event in the FSR tail by $\pm 5\%$. The distributions obtained from the re-weighted events are used to estimate the uncertainty at each level.

The systematic uncertainties that could arise from imperfections in the alignment are studied using MC samples with different assumed tracker reconstruction geometries (basic distortions)

based on the cylindrical symmetry of the tracker system [30]. These uncertainties are estimated using samples reconstructed with different basic distortions and in each case repeating the Tracker alignment procedure. The difference between the ideal geometry and the other scenarios is evaluated by comparing the A_{FB} values obtained in each case. The maximum of the alignment uncertainties calculated using each type of different geometry is taken as the alignment uncertainty for the corresponding M-Y bin.

The errors obtained from the χ^2 fits used to obtain the energy scale factors are used to modify the energy scale and calculate the associated uncertainties in the di-electron channel. In the di-muon channel, no energy scale factors are applied, but to estimate a possible scale uncertainty, the events are weighted by modifying the energy scale by 0.1%. The resulting differences with respect to the nominal asymmetry values are taken as the systematic uncertainties. No resolution uncertainty is accounted in the di-muon channel. The largest error from the χ^2 fits in the di-electron channel is 0.5% and this value is used to estimate the systematic uncertainty due to electron energy resolution.

The efficiency and pile-up uncertainties are estimated by comparing the results from the weighted and the unweighted samples for both channels.

To determine the uncertainties arising from the predictions of different PDF sets, we follow the PDF4LHC working group's recommendation [31, 32]. It is known that at NLO the predictions of the PDF sets CTEQ (CT10) [24, 33], NNPDF2.0 [34], and MSTW [35] are more consistent within themselves compared to other PDF sets. At the NLO level, the recommendation from the PDF4LHC working group is to use CTEQ (CT10), NNPDF and MSTW which have been calculated from Tevtron and HERA data. These PDF sets are also provided for different $\alpha_s(M_Z)$ values. The spread in the predictions is calculated from the central values of each of the three sets and PDF+α_s uncertainties using the prescriptions of combining the errors from each group. The central values are taken to be the midpoints of these spreads and the uncertainties are the distances of the extremes of the predictions to the midpoints. For each set, events are simulated and re-weighted using the varied PDF sets at the hard scattering level. All the weights for NNPDF, MSTW, and CT10α_s are calculated with respect to the CT10 set which is the baseline set used for the current analysis. CT10 has 52, NNPDF 100 and MSTW has 40 eigenvector directions. Events are re-weighted for each event for each PDF variation. Using the re-weighted forward and backward di-lepton mass distributions, re-weighted A_{FB} values are calculated for each M-Y bin. The final uncertainties are combined in quadrature using the full predicted spread as described in [31, 32].

The systematic errors due to unfolding procedure are calculated using toy MC samples. The effect is negligible and found to induce a variation of at most 0.03 in the A_{FB} measurement.

Each of the systematic uncertainties individually induces a change in A_{FB} of at most 0.09.

6 Results and Conclusion

The measured and expected raw A_{FB} distribution for each M-Y bin are shown with the associated statistical and systematical uncertainties in Figure 1 for the muon and in Figure 2 for the di-electron channel. The raw A_{FB} distributions are calculated using the efficiency corrected, pile-up re-weighted and background-subtracted data. The unfolded and combined A_{FB} distributions at the Born level are displayed in Figure 3. The position of the A_{FB} within a mass bin is determined by the expected mean value of the mass distribution at the Born level. The measurement and the unfolding are made with the acceptance cuts of $p_T(\mu) > 20$ GeV and

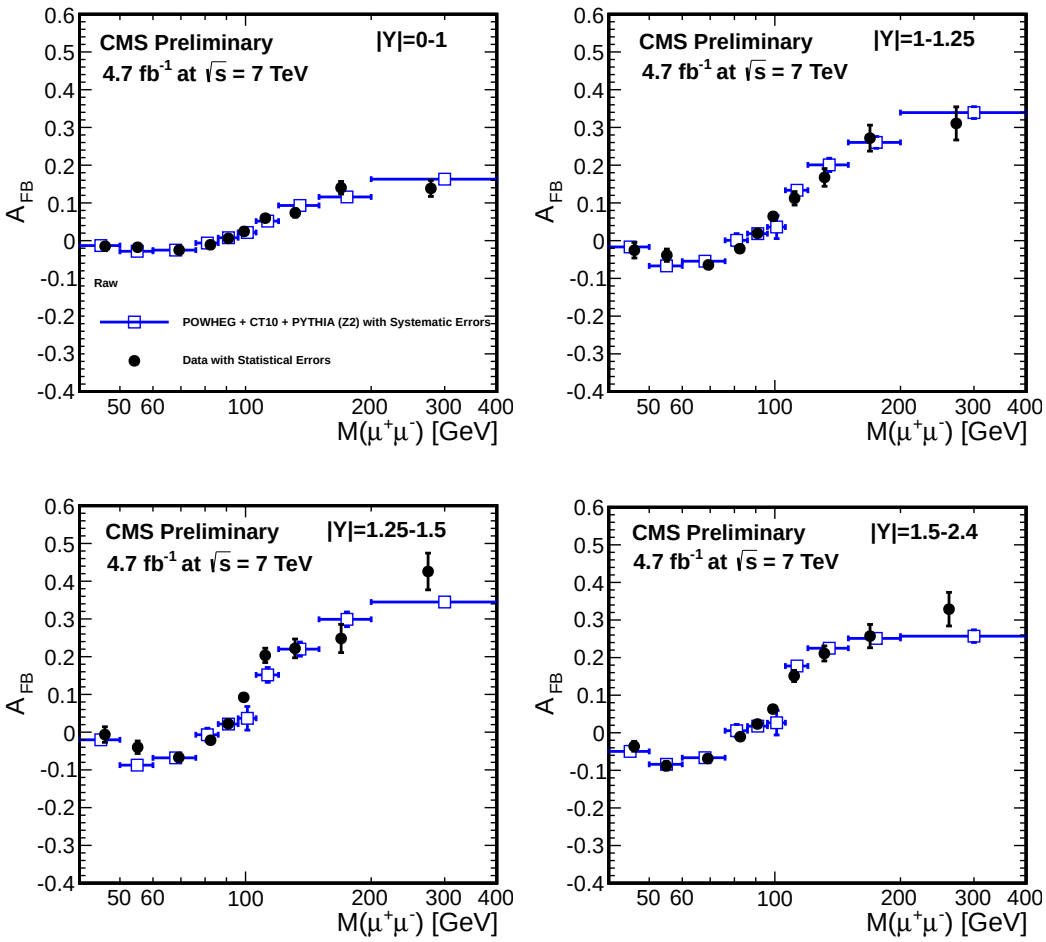

Figure 1: The raw A_{FB} measurement for the di-muon channel in different Y bins with the acceptance cuts of $p_T(\mu) > 20$ GeV and $|\eta(\mu)|$ <2.4. Data points are shown with the statistical error bars and the MC points with the total systematic error bars. The extent of the M error bars indicate the bin width. The raw A_{FB} is calculated using the efficiency corrected, pile-up re-weighted MC and background-subtracted data.

$|\eta(\mu)|$ <2.4. In the electron di-channel, unfolding also corrects for the gap in ECAL in the pseudo-rapidity range of $|\eta| = 1.444 - 1.566$.

We presented a measurement of the forward-backward asymmetry ($\mathrm{A_{FB}}$) for opposite charge lepton pairs produced via an intermediate $Z/\gamma*$ at $\sqrt{s}$ = 7 TeV in the CMS experiment based on an integrated luminosity of 4.7 fb^{-1}. We present $\mathrm{A_{FB}}$ as a function of the di-lepton mass for $\mathrm{M}_{\ell^+\ell^-} > 40$ GeV, the raw $\mathrm{A_{FB}}$ for both di-muons and di-electrons and the unfolded and combined measurement at the Born level. In conclusion, we find both the raw and the unfolded A_{FB} distributions to be consistent with the Standard Model predictions within the estimated uncertainties.

Acknowledgements

We wish to congratulate our colleagues in the CERN accelerator departments for the excellent performance of the LHC machine. We thank the technical and administrative staff at CERN

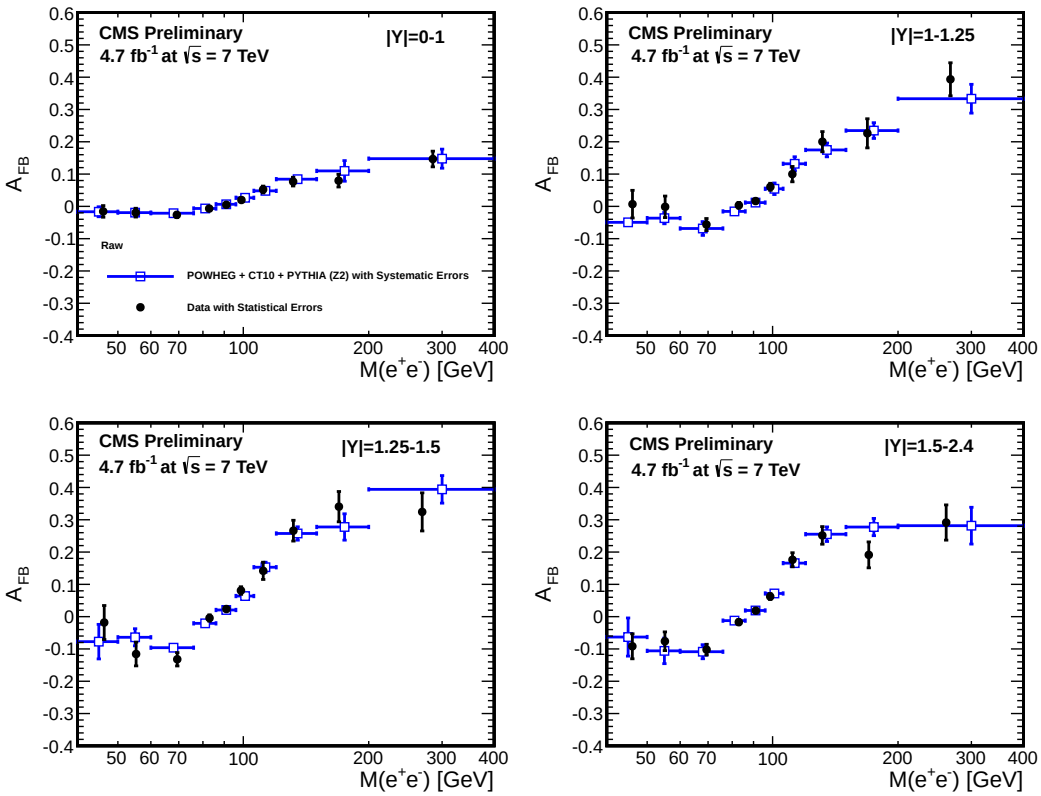

Figure 2: The raw A_{FB} measurement for the di-electron channel in different Y bins with the acceptance cuts of $p_T(e) > 20$ GeV and $|\eta(e)| <$2.4. Data points are shown with the statistical error bars and the MC points with the total systematic error bars. The extent of the M error bars indicate the bin width. The raw A_{FB} is calculated using the efficiency and mass resolution corrected, pile-up re-weighted MC and energy scale corrected and background-subtracted data.

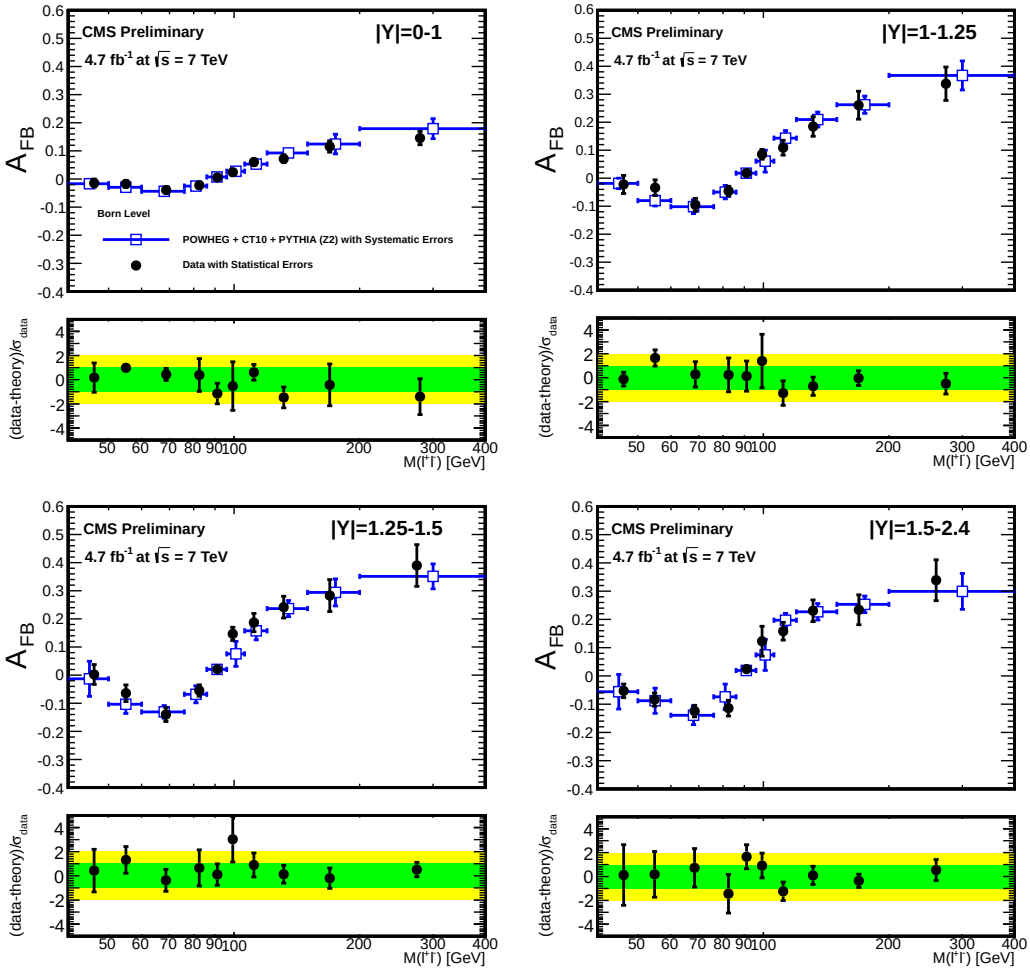

Figure 3: The combined ($\mu^+\mu^- + e^+e^-$) measurement of $A_{\rm FB}$ at the Born level in four Y bins with the acceptance cuts of $p_T(\ell) > 20$ GeV and $|\eta(\ell)|$ <2.4 (In the di-electron channel, unfolding also corrects for the gap in ECAL in the pseudo-rapidity range of $|\eta| = 1.444 - 1.566$.). Data points are shown with the statistical error bars and the MC points with the total systematic error bars. The extent of the M error bars indicate the bin width.

and other CMS institutes, and acknowledge support from: FMSR (Austria); FNRS and FWO (Belgium); CNPq, CAPES, FAPERJ, and FAPESP (Brazil); MES (Bulgaria); CERN; CAS, MoST, and NSFC (China); COLCIENCIAS (Colombia); MSES (Croatia); RPF (Cyprus); Academy of Sciences and NICPB (Estonia); Academy of Finland, MEC, and HIP (Finland); CEA and CNRS/IN2P3 (France); BMBF, DFG, and HGF (Germany); GSRT (Greece); OTKA and NKTH (Hungary); DAE and DST (India); IPM (Iran); SFI (Ireland); INFN (Italy); NRF and WCU (Korea); LAS (Lithuania); CINVESTAV, CONACYT, SEP, and UASLP-FAI (Mexico); MSI (New Zealand); PAEC (Pakistan); SCSR (Poland); FCT (Portugal); JINR (Armenia, Belarus, Georgia, Ukraine, Uzbekistan); MST, MAE and RFBR (Russia); MSTD (Serbia); MICINN and CPAN (Spain); Swiss Funding Agencies (Switzerland); NSC (Taipei); TUBITAK and TAEK (Turkey); STFC (United Kingdom); DOE and NSF (USA). Individuals have received support from the Marie-Curie programme and the European Research Council (European Union); the Leventis Foundation; the A. P. Sloan Foundation; the Alexander von Humboldt Foundation; the Belgian Federal Science Policy Office; the Fonds pour la Formation à la Recherche dans l'Industrie et dans l'Agriculture (FRIA-Belgium); the Agentschap voor Innovatie door Wetenschap en Technologie (IWT-Belgium); and the Council of Science and Industrial Research, India.

References

[1] D0 Collaboration, "Measurement of the Forward-Backward Charge Asymmetry and Extraction of $sin^2\theta_W^{eff}$ in $p\bar{p} \to Z/\gamma^* + X \to e^+e^- + X$ Events Produced at $\sqrt{s} = 1.96$ TeV", *Phys. Rev. Lett.* **101** (Nov, 2008) 191801. doi:10.1103/PhysRevLett.101.191801.

[2] D. London and J. Rosner, "Extra Gauge Bosons in E_6", *Phys. Rev. D* **34** (1986) 1530.

[3] J. Rosner, "Off-Peak Lepton Asymmetries from New Z's", *Phys. Rev. D* **35** (1987) 2244.

[4] M. Cvetic and S. Godfrey, "Electroweak Symmetry Breaking and New Physics at the TeV scale Barklow T L (ed.) et al.", *World Scientific* (1995) 383. arXiv:hep-ph/954216.

[5] J. Rosner, "Forward-backward asymmetries in hadronically produced lepton pairs", *Phys. Rev. D* **54** (1996) 1078. doi:10.1103/PhysRevD.54.1078.

[6] A. Bodek and U. Baur, "Implications of a 300-500 GeV/c^2 Z' boson on $p\bar{p}$ collider data at $\sqrt{s}$=1.8 TeV", *Eur.Phys.J.* **C21** (2001) 607–611. doi:10.1007/s100520100778. arXiv:hep-ph/0102160.

[7] CDF Collaboration, "Search for New Gauge Bosons Decaying into Dileptons in $\bar{p}p$ Collisions at $\sqrt{s}$ = 1.8 TeV", *Phys. Rev. Lett.* **79** (1997) 2192–2197. doi:10.1103/PhysRevLett.79.2192. Pillai, M., PhD. Thesis University of Rochester (1996).

[8] CDF Collaboration, "Limits on Quark-Lepton Compositeness Scales from Dileptons Produced in 1.8 TeV $p\bar{p}$ Collisions", *Phys. Rev. Lett.* **79** (1997) 2198. doi:10.1103/PhysRevLett.79.2198.

[9] H. Davoudiasl, J. Hewett, and T. Rizzo, "Phenomenology of the Randall-Sundrum Gauge Hierarchy Model", *Phys. Rev. Lett.* **84** (2000) 2080–2083. doi:10.1103/PhysRevLett.84.2080.

[10] CMS, "CMS technical design report, volume II: Physics performance", *J. Phys.* **G34** (2007) 995–1579. doi:10.1088/0954-3899/34/6/S01.

[11] R. Cousins, J. Mumford, and V. Valuev, "Measurement of Forward-Backward Asymmetry of Simulated and Reconstructed Z′→ $\mu^+\mu^-$ Events in CMS", *CMS Note* **2005/022** (2005).

[12] CMS Collaboration, "Measurement of Forward-Backward Asymmetry of Lepton Pairs and the Weak-mixing Angle at CMS", *CMS Phys. An. Summ. (PAS)* **EWK-10-010** (2011) http://cdsweb.cern.ch/record/1337272?ln=en.

[13] E. Yazgan, "Measurement of the Forward-Backward Asymmetry in Z/$\gamma*$ → $\mu^+\mu^-$ Events in CMS at 7 TeV", *Proc. Sci. (ICHEP 2010)* **035** (2010).

[14] E. Yazgan, "Measurement of the Forward-Backward Asymmetry in Z/$\gamma*$ → $\mu^+\mu^-$ Events in CMS at 7 TeV", *J. Phys. Conf. Ser.* **295** (2011) 012035. doi:10.1088/1742-6596/295/1/012035.

[15] J. Collins and D. Soper, "Angular Distribution of Dileptons in High-Energy Hadron Collisions", *Phys. Rev. D* **16** (1977) 2219. doi:10.1103/PhysRevD.16.2219.

[16] P. Fisher, U. Becker, and J. Kirkby, "Very high precision tests of the electroweak theory", *Phys. Lett.* **B356** (1995) 404–408. doi:10.1016/0370-2693(95)00714-V.

[17] M. Dittmar, "Neutral current interference in the TeV region: The experimental sensitivity at the CERN LHC", *Phys. Rev. D* **55** (1997) 161–166. doi:10.1103/PhysRevD.55.161. hep-ex:9606002.

[18] CMS Collaboration, "The CMS experiment at the CERN LHC", *JINST* **0803** (2008) S08004.

[19] CMS Collaboration, "CMS MUON Technical Design Report", *CERN/LHCC* **32** (1997).

[20] P. Nason, "A New Method for Combining NLO QCD with Shower Monte Carlo Algorithms", *JHEP* **11** (2004) 040. doi:10.1088/1126-6708/2004/11/040. arXiv:hep-ph/0409146.

[21] S. Frixione, P. Nason, and C. Oleari, "Matching NLO QCD Computations with Parton Shower Simulations: the POWHEG method", *JHEP* **11** (2007) 070. doi:10.1088/1126-6708/2007/11/070. arXiv:0709.2092.

[22] S. Alioli, P. Nason, C. Oleari et al., "NLO Vector-Boson Production Matched with Shower in POWHEG", *JHEP* **07** (2008) 06. doi:10.1088/1126-6708/2008/07/060. arXiv:0805.4802.

[23] T. Sjostrand, S. Mrenna, and P. Skands, "PYTHIA 6.4 Physics and Manual", *JHEP* **05** (2006) 026. arXiv:hep-ph/0603175.

[24] H.-L. Lai, M. Guzzi, J. Huston et al., "New parton distributions for collider physics", *Phys. Rev. D* **82** (Oct, 2010) 074024. doi:10.1103/PhysRevD.82.074024.

[25] J. Alwall, P. Demin, S. de Visscher et al., "MadGraph/MadEvent v4: The New Web Generation", *JHEP* **09** (2007) 028. doi:10.1088/1126-6708/2007/09/028. arXiv:0706.2334.

[26] N. Davidson, G. Nanava, T. Przedzinski et al., "Universal Interface of TAUOLA Technical and Physics Documentation", arXiv:1002.0543.

[27] J. Sulkimo, M. Takahata, S. Tanaka et al., "Geant 4 – A Simulation Toolkit", *NIM A* **506/3** (2003) 250–303. doi:doi:10.1016/S0168-9002(03)01368-8.

[28] J. Allison, K. Amako, J. Apostolakis et al., "Geant4 developments and applications", *IEEE Transactions on Nuclear Science* **53/1** (2006) 270–278. doi:10.1109/TNS.2006.869826.

[29] S. Baffioni et al., "Electron reconstruction in CMS", *Eur. Phys. J.* **C49** (2007) 1099–1116. doi:10.1140/epjc/s10052-006-0175-5.

[30] CMS Collaboration, "Alignment of the CMS Silicon Tracker during Commissioning with Cosmic Rays", *JINST* **5** (2010) T03009, arXiv:0910.2505. doi:10.1088/1748-0221/5/03/T03009.

[31] M. Botje et al., "The PDF4LHC Working Group Interim Recommendations", arXiv:1101.0538.

[32] S. Alekhin et al., "The PDF4LHC Working Group Interim Report", arXiv:1101.0536.

[33] P. M. Nadolsky, H.-L. Lai, Q.-H. Cao et al., "Implications of CTEQ global analysis for collider observables", *Phys. Rev. D* **78** (Jul, 2008) 013004. doi:10.1103/PhysRevD.78.013004.

[34] R. D. Ball et al., "A first unbiased global NLO determination of parton distributions and their uncertainties", *Nucl. Phys.* **B838** (2010) 136–206, arXiv:1002.4407. doi:10.1016/j.nuclphysb.2010.05.008.

[35] A. D. Martin, W. J. Stirling, R. S. Thorne et al., "Parton distributions for the LHC", *Eur. Phys. J.* **C63** (2009) 189–285, arXiv:0901.0002. doi:10.1140/epjc/s10052-009-1072-5.